6

Electric field sensing schemes using low-coherence light and $LiNbO_3$ electrooptical retarders

Celso Gutiérrez-Martínez
Instituto Nacional de Astrofísica, Optica y Electrónica (INAOE)
México

1. Introduction

Electric fields sensing and measurement of high and low intensity fields coming either from natural phenomena, or from human activities is an important subject as it impacts the daily activities in industrial and commercial environments around the world. Static and dynamic electric fields are produced by different sources including electric power equipment, power generation and distribution facilities, high voltage transmission lines, telecommunication equipments, electromagnetic interference, human medical signals, etc. The detection and measurement of electric fields are important tasks as they are related to safety of equipments and personnel and even health of people.

More common electric field meters use conductive electrodes linked by cables to the measuring electronics and very often such arrangements distort the unknown field. Different techniques and apparatus for the measurement of either extremely high or extremely low electric fields are reported in the technical literature (Johnston et al, 1986; Kirkham, 2006).

Using optical techniques are very promising and are being explored, aiming to minimize distortion and interference on electric field measurements. Optical techniques use light to sense electric fields taking advantage of their interaction in electro-optic crystals. Additionally, as the optical techniques disturb minimally the electric fields and are inherently immune to electromagnetic interference, a wide variety of electric field sensing schemes using electro-optic devices have been tested up to date. Most of such schemes use the Pockels effect either in bulk or in integrated optics Lithium Niobate (LiNbO3) devices. Polarization and Mach-Zehnder interferometers are being used as electric field sensors.

Sensor devices either using electrodes or electrode-less can be studied and integrated on sensing schemes. Using electrodes on the sensing devices gives a high sensitivity but the main disadvantage is that the electrodes may disturb the measured electric field. Such schemes are very well adapted to measure low intensity electric fields (mV/m to hundreds V/m) as found in telecommunication systems and electronic apparatus (Meier et al, 1994; Rao et al, 1999; Yim et al, 1998; Lee et al, 2006). Electrode-less sensors disturbs minimally the measured field but the sensitivity is relatively low and such devices are better adapted to

the measurement of high intensity fields ranging from some kV/m to hundreds of kV/m (4 to 2000 kV/m), as found in natural lightning strikes, high power electrical facilities and high voltage transmission lines (Johnston et al, 1986; Kirkham, 2006).

In an electric field sensing scheme based on the electro-optic interaction between light, the electric field modulates the intensity of an optical beam passing through an electro-optic bulk crystal or optical waveguide. The modulated light can be transmitted through optical fiber channels or even over free space optical links.

Optical intensity modulators can be implemented by two-wave interferometers such as polarization or Mach-Zehnder. Mach-Zehnder modulators have been widely studied and reported as electric field sensors based on intensity modulation of light (Meier et al, 1994; Rao et al, 1999; Yim et al, 1998; Lee et al, 2006; Hidaka and Fujita, 1982; Naghski et al, 1994; Cecelja et al, 2001).

In an alternative approach, electric fields can be sensed by schemes associating low-coherence optical sources and electro-optical polarization interferometers, which in this case, introduce optical delays. The sensed electric field modulates an optical delay, instead of the optical intensity. The modulation of optical delays is well known as optical coherence modulation (Delisle & Cielo, 1975; Brooks and Wentworth, 1985; Chu & Dickey, 1991; Bock & W. Urbanczyk, 2000).

In coherence modulation of light, electric fields are imprinted on light as a sequence of optical delays, provided they are greater than the coherence time of the optical source. Coherence modulation of light uses electro-optic retarders and practical realizations are based on lithium niobate (LiNbO3) electro-optic technology (Porte & Goedgebuer, 1992; Gutiérrez-Martínez et al, 1995). A sensing scheme can be implemented using fiber optics components and electrode-less LiNbO3 electro-optic retarders. The demodulation of the sensed electric field is realized directly by scanning Michelson interferometry or by a fiber or integrated optics two-wave interferometer, when sensor and demodulator are matched at the same optical delays.

Electric field sensing implementation using coherence modulation of light is described in this chapter. Experiments of sensing high intensity and wide band electric fields, using electrode-less optically matched electro-optical retarders are described. Electric field detection using such a technique has been previously reported describing the detection of 60 Hz electric fields (Rodríguez-Asomoza & Gutiérrez-Martínez, 2001; Gutiérrez-Martínez et al, 2002; Gutiérrez-Martínez & Santos-Aguilar, 2004). Wider band, up to 20 kHz has been also was successfully tested by detecting high intensity electric fields, ranging from 20 to 350 kVpp/m [22-23](C. Gutiérrez-Martínez et al, 2007; Gutiérrez-Martínez & Santos-Aguilar, 2008).

A very attractive feature of coherence modulation is that it allows serial or parallel multiplexing of optical delays (Goedgebuer et al, 1987; Goedgebuer & Hamel, 1987; Gutiérrez-Martínez et al, 1997.) and, from this fact, multi-point sensing arrays can be proposed. Serial coherence multiplexing can be a promising technique in fibred schemes for distributed sensing arrays as several optical delays can be cascaded over a single optical channel.

2. Coherence modulation operating principle

To recall the operating principle, the block diagram of an integrated optics electric field sensor system, based on coherence modulation of light, is shown in figure 1. The system includes a low-coherence optical source, an electro-optic sensor (optical retarder), an optical fiber channel and a receiver module, which is implemented by a second optical retarder (either integrated optics or a fiber passive interferometer) as coherence demodulator, and a photo-detector.

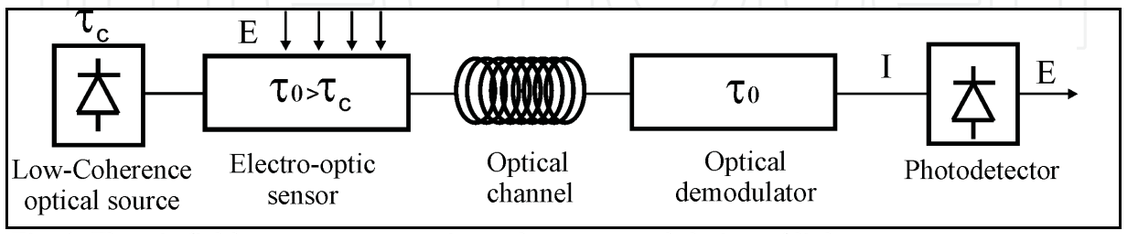

Fig. 1. Electric field sensor system using coherence modulation of light

According to the block diagram, light coming from a low-coherence optical source is injected into the electro-optic sensor, which introduces an optical delay τ_0, greater than the source coherence time τ_c. In this model, when low-coherence light $s(t)$ is delayed, the light at the output of the optical retarder is given as (Gutiérrez-Martínez, 1994)

$$s_o(t) = \frac{1}{2}s(t) + \frac{1}{2}s(t-\tau_o) \tag{1}$$

The detected optical intensity at the output of the demodulator is now

$$I_m = < s_O^*(t)s_O(t-\tau_0) > = \frac{1}{4}\left|s(t)\right|^2 + \frac{1}{4}\left|s(t-\tau_0)\right|^2 + \frac{1}{4}\left\{\left\langle s(t-\tau_0)s^*(t)\right\rangle + \left\langle s^*(t-\tau_0)s(t)\right\rangle\right\}$$
$$= \frac{1}{2}P_0 + \frac{1}{2}\mathrm{Re}\left\{G(\tau_0)\right\}$$

P_0 is the average optical power from the source and $G(\tau_0)$ is the autocorrelation function. The transmitted optical intensity for the normalized real part of $G(\tau_0)$ is given as

$$I_m = \frac{P_0}{2}\left\{1 + |g(\tau_0)|\cos\left(2\pi\frac{1}{\lambda_0}v\tau_0\right)\right\} \tag{2}$$

λ_0 is the center optical wavelength and v is the light propagation velocity.

From expression (2), one finds that optical interference will exist on depending on the superposition of two delayed waves, in the range of the optical coherence, e.g. when the optical delay is shorter than the coherence time or equivalently, when the optical path-difference (OPD), is shorter that the coherence length. As the optical delay is longer than the coherence time, the optical interference disappears and the optical intensity becomes $\frac{P_0}{2}$, figure 2.

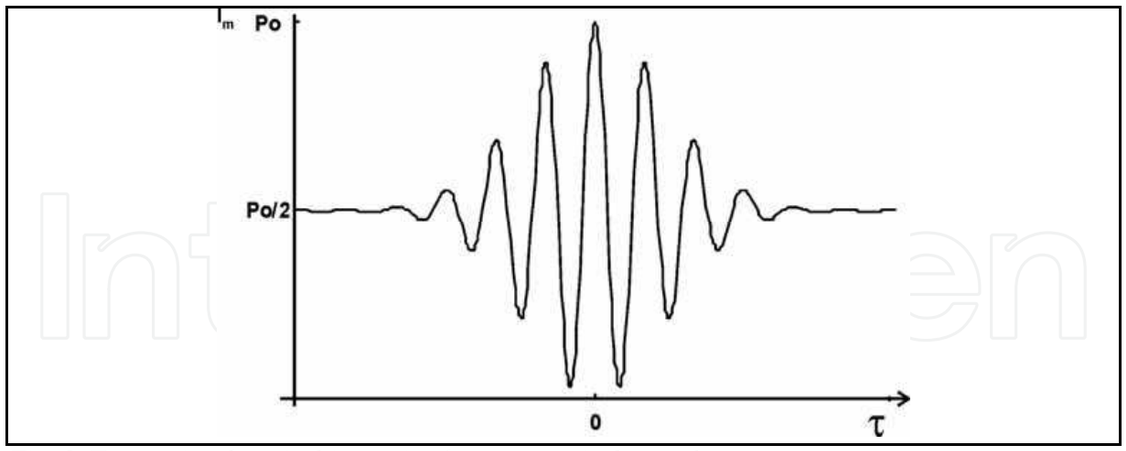

Fig. 2. Transmitted optical intensity from an optical retarder.

An optical delay can be dynamically modulated by an information signal thus becoming an optical information carrier. The modulated signal is centered on a static optical delay (or optical path-difference) and the modulation process is optimal when the static delay is longer than the coherence time.

As shown in figure 1, the demodulation process can be achieved using the same operating principle; e. g. by introducing a second optical delay or optical path-difference (OPD), which is matched to the same value on the first retarder (modulator). Such a situation allows that the two delayed waves interfere mutually. When detecting the optical interference, a photodetector delivers an average optical power.

The optical signal from the electrooptic sensor can be expressed as

$$s_O(t) = \frac{1}{2}s(t - \frac{\tau_0}{2}) + \frac{1}{2}s(t + \frac{\tau_0}{2}) \tag{3}$$

If the optical demodulator introduces a second delay τ_d; its output optical signal $s_d(t)$ is

$$s_d(t) = \frac{1}{2}s_o(t - \frac{\tau_d}{2}) + \frac{1}{2}s_o(t + \frac{\tau_d}{2}) \tag{4}$$

The detected optical intensity at the output of the demodulator is now

$$\begin{aligned} I_d &= < s_d^*(t) s_d(t) > \\ &= \left\langle \left[\frac{1}{2}s_o^*(t - \frac{\tau_d}{2}) + \frac{1}{2}\, s_o^*(t + \frac{\tau_d}{2}) \right] \left[\frac{1}{2}s_o(t - \frac{\tau_d}{2}) + \frac{1}{2}s_o(t + \frac{\tau_d}{2}) \right] \right\rangle \\ &= \frac{P_0}{4} + \frac{P_0}{4}g(\tau_0) + \frac{P_0}{4}g(\tau_d) + \frac{P_0}{8}g(\tau_d - \tau_0) + \frac{P_0}{8}g(\tau_d + \tau_0) \end{aligned} \tag{5}$$

The detected optical intensity can be expressed in terms of the optical path-differences $d = v\tau_d$, $d_{mo} = v\tau_o$; v is the light propagation speed and as $g(\tau_0) \approx 0$, such an intensity becomes

$$I_d(d) = \frac{1}{4}P_0 + \frac{P_0}{4}g(d) + \frac{P_0}{8}g(d - d_{m0}) + \frac{P_0}{8}g(d + d_{m0}) \tag{6}$$

Eq. 6 represents the autocorrelation function of the delayed light, showing the fringe pattern at the output of the optical demodulator when the optical path difference is scanned between $-d_{m0}$ through $+d_{m0}$, as depicted in figure 3.

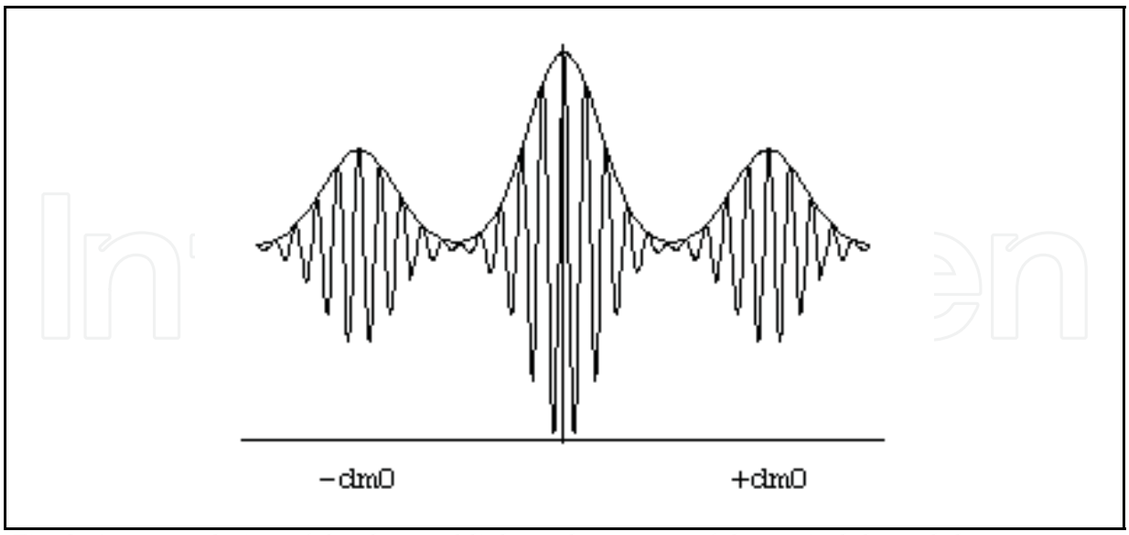

Fig. 3. Autocorrelation of the detected light at the output of the optical demodulator

Based on the previously described operating principle, an information signal can be transmitted using the optical path-difference $d_m = d_{m0} + \Delta d(t)$, as a modulated carrier. To recuperate the information, the optical demodulator will be tuned to $d \cong d_{m0}$.

$$I_d(d \cong d_{m0}) = \frac{1}{4}P_0 + \frac{P_0}{4}g(d_{m0}) + \frac{P_0}{8}g(d_{m0} - d_{m0}) + \frac{P_0}{8}g(d_{m0} + d_{m0})$$

Finally, as $d_{m0} >> l_c$, the detected optical intensity at the output of the coherence demodulator is

$$I_d(d \cong d_{m0}) = \frac{1}{4}P_0 + \frac{P_0}{8}g(d_{m0} - d_{m0} - \Delta d(t)) \tag{7}$$

An electric signal $E(t)$ can modulate the optical path-difference and, at the demodulator, the electric field can be detected as an intensity variation on the autocorrelation of the received light. The variation is the strongest when the optical path-differences on the modulator and the demodulator are perfectly matched.
The modulated optical path-difference is

$$d_m = d_{m0} + KE(t) \tag{8}$$

d_{m0} is the static optical path-difference, $KE(t)$ is the dynamic variation by the electric field and K is the modulator sensitivity. The electric field is recuperated by matching the static path-differences at d_{m0}.

$$I_d = \frac{P_0}{4} + \frac{P_0}{8}g(d_{m0} - d_{m0} + KE(t))$$

If $KE(t) \ll d_{m0}$, then from eq. 2, $g(d_{m0} - d_{m0} + KE(t)) = |g(0)|\cos(2\pi\frac{1}{\lambda_0}KE(t))$ and as $|g(0)| = 1$,

$$I_d = \frac{P_0}{4} + \frac{P_0}{8}\cos(2\pi\frac{1}{\lambda_0}KE(t)) \tag{9}$$

The dynamic variation on the detected optical intensity is depicted by figure 4.

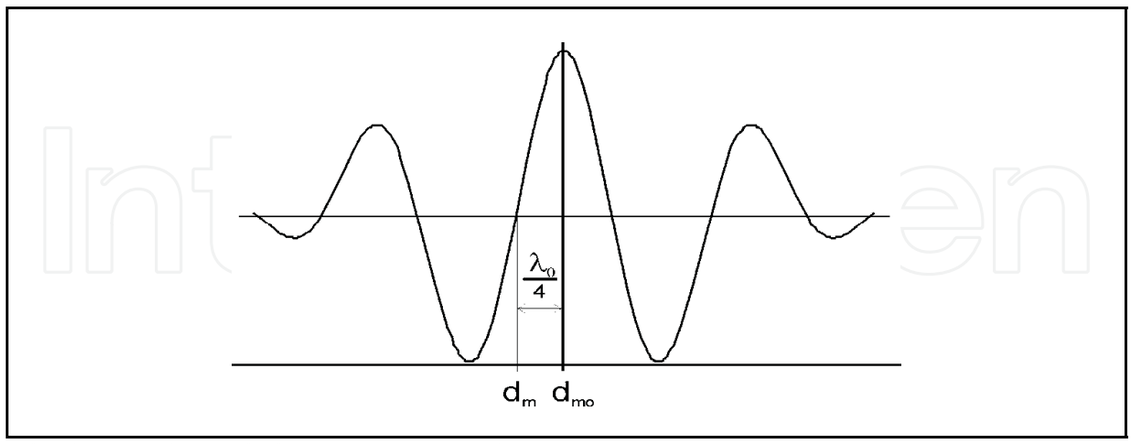

Fig. 4. Intensity variation at the output of the matched optical demodulator

As shown in figure 4, a linear detection of the modulating electric field can be achieved by shifting the static optical path-difference to

$$d_m = d_{m0} - \frac{\lambda_0}{4} + KE(t) \tag{10}$$

Eq. 10 can be substituted in Eq. 9, giving

$$I_d = \frac{P_0}{4} + \frac{P_0}{8}\cos\left(\frac{2\pi}{\lambda_0}KE(t) - \frac{\lambda_0}{4}\right) \tag{11}$$

Or, equivalently

$$I_d = \frac{P_0}{4}\left[1 + \frac{1}{2}\ s\sin\left(2\pi\frac{1}{\lambda_0}KE(t)\right)\right] \tag{12}$$

The range between the maximum and minimum of I_d determines the half-wave voltage $E_\pi = \frac{\lambda_0}{2K}$

Eq. 12, becomes then

$$I_d = \frac{P_0}{4}\left[1 + \frac{1}{2}\sin\left(\frac{\pi}{E_\pi}E(t)\right)\right] \tag{13}$$

Now when $E(t) << E_\pi$

$$I_d = \frac{P_0}{4}\left[1 + \frac{1}{2}\ \frac{\pi}{E_\pi}E(t)\right] \tag{14}$$

When $E(t)$ is small, the detected optical intensity is linear around $d_{mo} \pm \frac{\lambda_0}{4}$.

The generation of optical delays can be achieved by means of two-wave interferometers such as Michelson, Mach-Zehnder and polarization (Gutiérrez-Martínez, 1994).
The Michelson interferometer, consists of two mirrors, which are illuminated by a split optical beam coming from the same optical source. The mirrors are placed at distances

d_1 and d_2 from the beam splitter. If v is the light propagation velocity, the optical delay is $\tau = \frac{2(d_2 - d_1)}{v}$.

The Mach-Zehnder interferometer consists of two mirrors and two optical splitters. Light follows two separate identical paths. One path is modified by an optical slab of thickness e and refractive index n_e, thus introducing an optical delay $\tau = \frac{2(n_e - 1)e}{v}$.

The polarization interferometer consists of a birefringent optical waveguide, exhibiting ordinary n_o and extraordinaire n_e refractive index and length L. The optical waveguide is located between optical polarizers. The introduced optical delay is given as $\tau = \frac{(n_o - n_e)L}{v}$.

In the remainder of this chapter, polarization interferometers are the main studied devices. Such devices can be easily implemented either by birefringent optical waveguides or polarization maintaining optical fibers (PMF), although autocorrelation of light and measurement of optical path-differences are easily realized by scanning Michelson interferometry.

3. Coherence modulation based on LiNbO3 electrooptic crystals and waveguides.

In coherence modulated schemes, light emitting diodes (LED), superluminiscent diodes (SLD) and multi-longitudinal laser diodes (MLLD), are well adapted as those devices provide low coherence light. The optical delays are easily generated by lithium niobate ($LiNbO_3$) electro-optic waveguides, acting as polarization interferometers. Such devices generate static optical delays (or equivalently, optical path-differences, OPD's), which can be modulated by an electric field. The optical retarders often used are Z-cut Y-propagating LiNbO3 birefringent optical waveguides, which introduce optical delays as 45° polarized light is projected in orthogonal propagating modes TE and TM (Rodríguez-Asomoza & Gutiérrez-Martínez, 2001). Such modes travel in the waveguide at different velocities, as determined by the ordinary and extraordinary refractive index difference $(n_o - n_e)_g$ =0.083 at λ_0 =1310 nm. An optical waveguide acting as an optical retarder (coherence modulator) is depicted in figure 5.

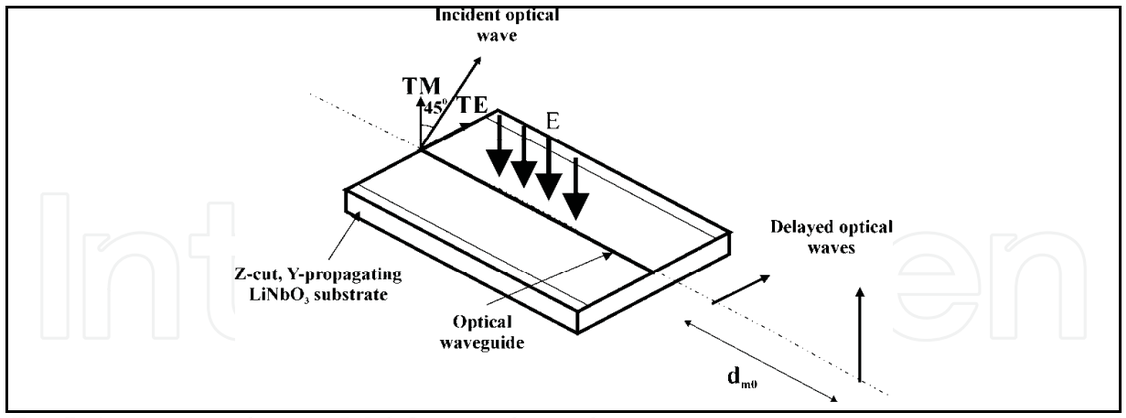

Fig. 5. An integrated optics $LiNbO_3$ optical retarder

In agreement to the theoretical principles in the previous section, the optical delay between the orthogonal waves TE and TM is given as

$$\tau_0 = \frac{(n_o - n_e)_g L}{v}$$

L is optical waveguide length and v is the light propagation velocity in the waveguide. The corresponding static OPD is then

$$d_{m0} = \tau_0 v = (n_o - n_e)_g L \tag{15}$$

When an electric field $E_z(t)$ is sensed by the coherence modulator, it induces a dynamic variation $\Delta d(t)$ on the optical path-difference. On a z-cut $LiNbO_3$ birefringent waveguide, the electric field is oriented on the Z-axis of the crystal, taking advantage of the linear electro-optic coefficients r_{13} and r_{33}. The time-varying optical path-difference is then given as

$$d_m(t) = d_{m0} + \Delta d(t) \tag{16}$$

From expression (14), $\Delta d(t) = \frac{\lambda_0}{2}\frac{E_z(t)}{E_\pi}$, E_π is the half-wave electric field given as

$$E_\pi = \lambda_0 \Big/ \left(r_{33} n_e{}^3 \Gamma_{TM} - r_{13} n_o{}^3 \Gamma_{TE}\right) L \tag{17}$$

According to expression (17), L represents the interaction length between the electric field and the optical wave, r_{13} and r_{33} are the electro-optic coefficients, Γ_{TE} and Γ_{TM} are the electric-optical overlapping coefficients and λ_0 is the center wavelength of the optical source. The half-wave electric field depends mainly on the length of the electro-optics sensor. A basic sensing scheme based on matched optical path-differences and coherence modulation of light is shown in figure 6.

In this scheme, the electric field sensor is an optical waveguide on an $LiNbO_3$ electrooptic crystal. The sensed electric field is imprinted in the optical path-difference given by eq. (16). The optical signal is transmitted through the optical channel. The coherence demodulator is a two-wave interferometer which will introduce a second optical path-difference. The modulating electric field will be recuperated when the path-differences are optically matched. The coherence demodulator can be implemented either by a second optical

waveguide or by a fiber passive interferometer. This last device is easily implemented by segments of polarization-maintaining fiber (PMF).
At the output of the optical demodulator, in agreement to expression 6, optical interference exists when the optical path-differences are matched.

$$I_r(d_{m0}) = \frac{P_0}{4} + \frac{P_0}{8} g(d_{m0})$$

And from expression 13, the optical intensity is given as

$$I_r(t) = \frac{P0}{4} + \frac{P_0}{8} sen(\pi \frac{Ez(t)}{E_\pi})$$

Additionally, if $Ez(t) << E_\pi$, from eq. 14, the measured optical power is

$$Pr(t) = \frac{P0}{4}\left(1 + \frac{\pi}{2}\frac{E_z(t)}{E_\pi}\right) \tag{18}$$

This last expression represents an intensity modulation and the electric field is then detected as a linear variation of the received optical power.

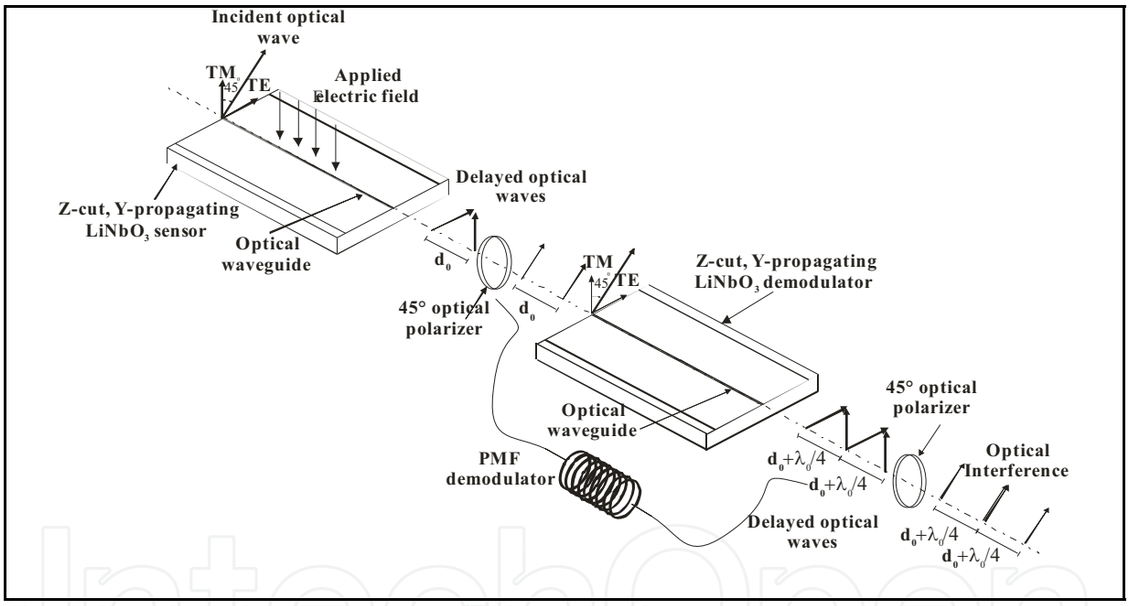

Fig. 6. Optical matching in an electric field sensing scheme.

4. Elecrooptic sensors characterization

4.1 Optical Transfer Function and half-wave electric field

The optical transfer function of an $LiNbO_3$ sensor relates the optical output power and the sensed electric field. The transfer function is determined by sensing DC electric fields, which modulate the light traveling through the sensing optical waveguide, as shown in figure 7.
When the optical waveguide is used as a dielectric sensor, no electrodes are associated to the crystal and the electric field is present in the dielectric environment surrounding it (most commonly air $\varepsilon r = 1$).

The uniform electric field E_1, in the air, finds a boundary condition and hence a discontinuity on the surface of the electro-optic sensor. The discontinuity is determined by the crystal permittivity, $\varepsilon_r = 35$ (Gutiérrez-Martínez & Santos-Aguilar, 2008). As the electric field is perpendicular to the crystal surface and considering the boundary conditions, the optical waveguide senses a uniform electric field E_2, given as (Ulaby, 2000).

$$E_2 = \frac{\varepsilon_{r1}}{\varepsilon_{r2}} E_1 \tag{19}$$

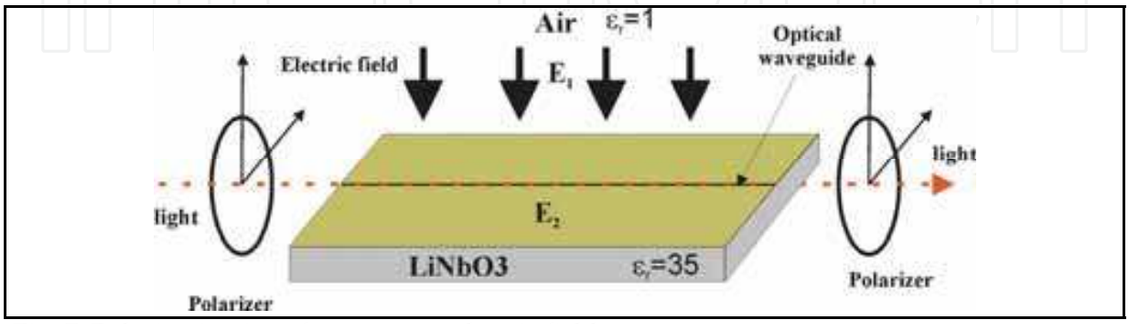

Fig. 7. Polarization interferometer as electric field sensor

After sensing-detection, the electro-optic transfer function given by eqs. 18 and 19, becomes

$$Pr(t) = \frac{P_0}{4}\left(1 + \frac{\pi}{2}\frac{E_2}{E_\pi}\right) \tag{20}$$

From eq. 17, the half-wave electric fields (E_π), for L=10, 30 and 60 mm $LiNbO_3$ electrooptic sensors, at λ_0=1310 nm, are = 430, 144 and 72 kVpp/m, respectively.
The optical transfer function for a 36 mm $LiNbO_3$ sensor has been calculated and measured at the output of the coherence demodulator for a DC electric field ranging between 0-330 kVpp/m. The optical transfer function is shown in figure 8.

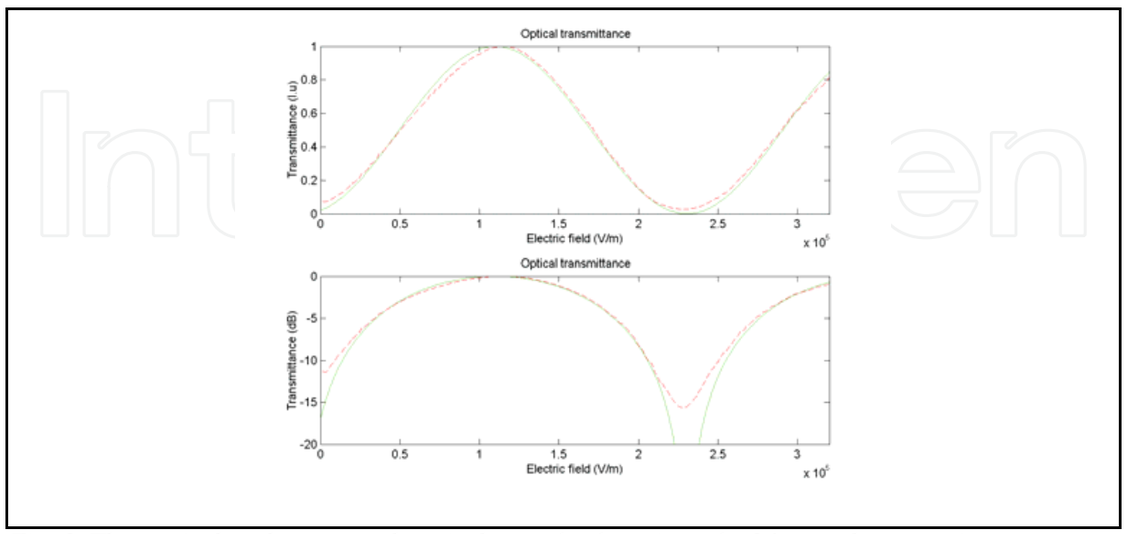

Fig. 8. Theoretical and measured optical transfer function of a 36 mm electrooptic sensor

In this figure, the upper graph shows a continuous curve corresponding to linear-scale measurement; the theoretical optical transfer is shown in dashed lines. The lower graph shows the transfer function in logarithmic scale. The measured half-wave electric field is of about 112 kVpp/m, in good agreement to the theoretical 120 kVpp/m, given by eq. 17. On the linear-scale, the optical transfer function shows a sinusoidal shape in agreement to eq. 13 and the regions of linear response can be identified. A first linear region is around 50 KV/m; a second one is at around 175 kVpp/m and so on. Linear sensing of electric fields can be considered, depending on the field intensity ranges.

4.2 Optical correlation and path-differences

To implement a coherence modulation electric field sensing system, the static optical path-differences of coherence modulators and demodulators, must be firstly determined. A straightforward way to measure the optical autocorrelation and optical path-differences is by using a Scanning Michelson Interferometer (SMI) (Gutiérrez-Martínez et al, 2000), figure 9(a).

The measurement set-up is based on a super-luminescent diode (SLD) exhibiting a coherence length of about 60 μm. The electric field sensor is an $LiNbO_3$ coherence modulator. The SMI measures the autocorrelation of the transmitted light. The light is photodetected, amplified and the output voltage, corresponding to the received optical intensity, is digitized for further data processing. Figure 9(b) shows the auto-correlation fringe pattern of a coherence electrooptic sensor exhibiting a static optical-path-difference d_0 = 1.57 mm, corresponding to a physical length of 19 mm. The SMI can itself, be useful to detect a sensed electric field when adjusting it to the sensor optical path-difference.

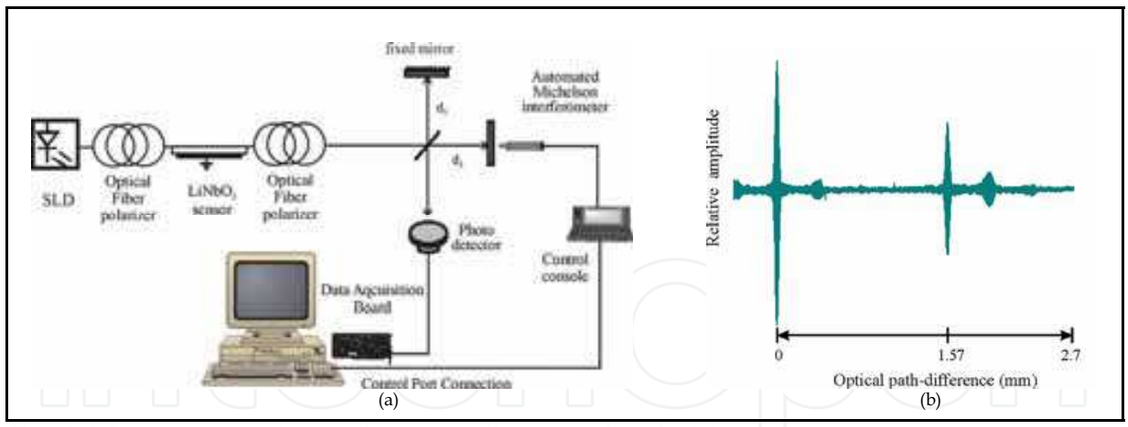

Fig. 9. Measurement of optical autocorrelation and path-differences.

5. Implementing experimental electric field sensing schemes

In the frame of this chapter, the implementation of an experimental electric field sensing scheme is described in this section, figure 10.

The experimental system includes a super-luminescent diode (SLD), emitting at λ_0 = 1 310 nm, with a coherence length of about 60 μm and an average emitted power of 500 μWatts. The electric field sensor is a fiber pigtailed Z-cut Y-propagating LiNbO3 integrated optics

coherence modulator, which introduces a static OPD d_{m0}. The optical demodulator has been implemented in two ways:

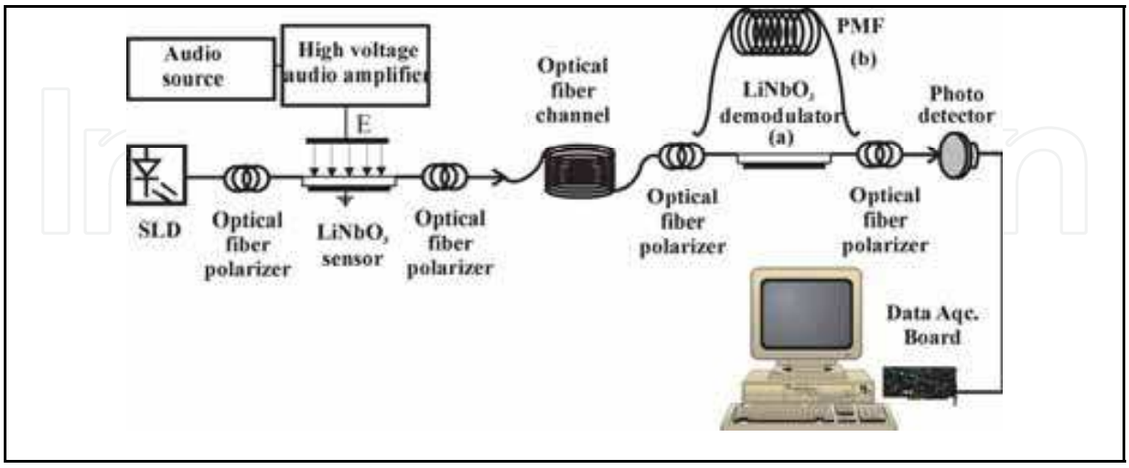

Fig. 10. Experimental electric field sensing system.

1. A pigtailed electro-optic birefringent optical waveguide, acting as a two-wave interferometer, matched to the sensor's OPD, insert (a) in figure 10.
2. An all fiber two-wave interferometer, implemented using polarization maintaining optical fiber (PMF), also matched to the electro-optic sensor, insert (b) in figure 10.

The 45° optical fiber polarizers ensure the propagation of TE and TM optical modes on the electro-optic birefringent waveguides, thus introducing OPD's.

A 700 m-optical fiber channel completes the experimental set-up.

To implement the electric field sensing system, the static optical path-differences of the coherence sensor and the optical demodulators were measured.

In a first case, two identical 13 mm-length birefringent optical waveguides were used. As it can be observed on figure 11(a), the electro-optic crystals exhibit identical static optical-path-differences around d_{m0} =1 mm. The figure shows the overlapping of the OPD's on the sensor and demodulator crystals, when both devices are cascaded and the transmitted light is measured by a scanning Michelson Interferometer. Figure 11(b) corresponds to a second case, when an $LiNbO_3$ sensor (13.2 mm-length), is matched to a PMF two-wave interferometer. The fiber interferometer has been implemented using 3.45 m of 3M FS-CG-6121 PMF. In this second case, the optical path-difference is of about d_{m0} =1.1 mm and the crystal and fiber demodulator are also well matched. A main advantage, when using a PMF demodulator, is that the photodetected signal is stronger, thus ensuring a higher signal to noise ratio. To achieve a linear detection of the optical signal, the demodulators (electrooptic crystal and PMF) were designed to introduce an OPD $(d_{m0} \pm \frac{\lambda_0}{4})$; however, ($\frac{\lambda_0}{4}$ =325 nm) is a very small length and it is difficult to define it accurately when constructing and polishing the crystal or fiber optical faces.

After setting-up the two electro-optic sensor schemes, figures 11(a) and 11(b) show the measured matched OPD's. As it can be observed, the electro-optic sensors exhibit static optical-path-differences around d_{m0} = 1 and 1.1 mm, respectively. A zoom of the

interference fringes around 1 mm gives a more accurate measurement, thus confirming that interference exists only in the range of the coherence length of the optical source and ensuring the demodulation of the sensed electric field. This represents an unequal feature of the implemented sensing schemes.

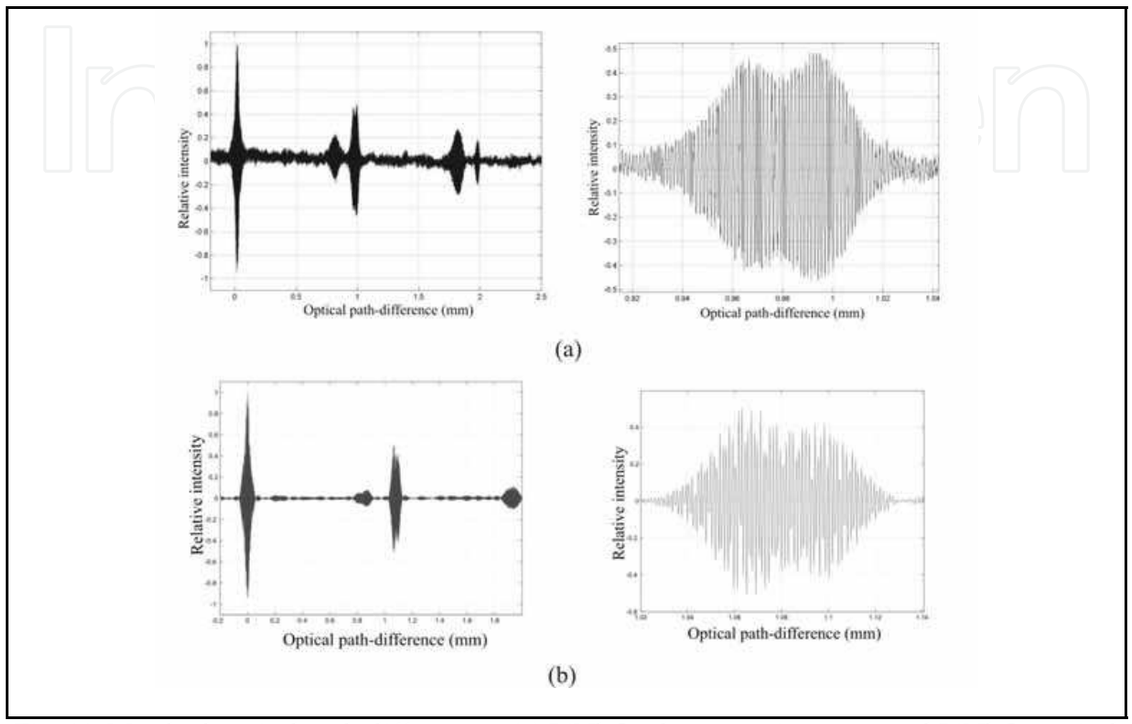

Fig. 11. Matched optical path differences: (a) $LiNbO_3$ electro-optic sensor and $LiNbO_3$ optical demodulator; (b) $LiNbO_3$ electro-optic sensor and PMF two-wave interferometer demodulator.

5.1 A wideband sensing scheme

To test the sensing scheme, a first experiment consisted in applying sinusoidal electric fields to the coherence electro-optic sensor, in a frequency band up to 20 kHz. The modulated light was then transmitted through the 700 m optical fiber channel. At the receiver, light was measured by the electro-optic coherence demodulator, already tuned around the static optical path-difference of 1 mm. The frequency response of the sensing scheme was limited by the bandwidth of a wide-area photodetector to 20 kHz. Such a response was measured resulting flat in the frequency range as depicted on figure 12(a). The electric field was generated by a signal generator and then amplified to a high voltage, which was applied to two parallel plates, not in contact with the electro-optic sensor, in order to generate a uniform electric field. A sinusoidal AC electric field, ranging between 10 and 350 kVpp/m was measured. The field sensing-detection process shows a good linearity in the range of 10-350 kVpp/m, as shown in figure 12(b).

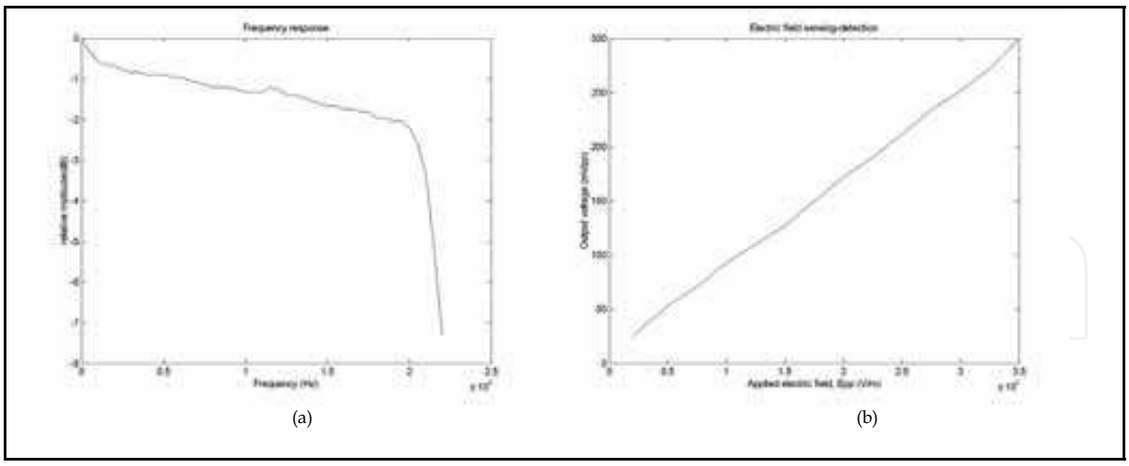

(a) (b)

Fig. 12. Frequency response of the electric field sensing scheme.

To illustrate the operation of the experimental set-up, high-intensity electric fields of different frequencies were measured. Figure 13 illustrates the input and output waveforms for electric fields of 200 kVpp/m and 100 Hz and 20 kHz respectively. In figure 13, the input signal corresponds to a 200 kVpp/m electric field and the output signal level is of 200 mVpp. The noise level is of about 2mVpp. The signal to noise ratio (SNR) of the recuperated signal corresponding to a 200 kVpp/m was better than 30 dB.

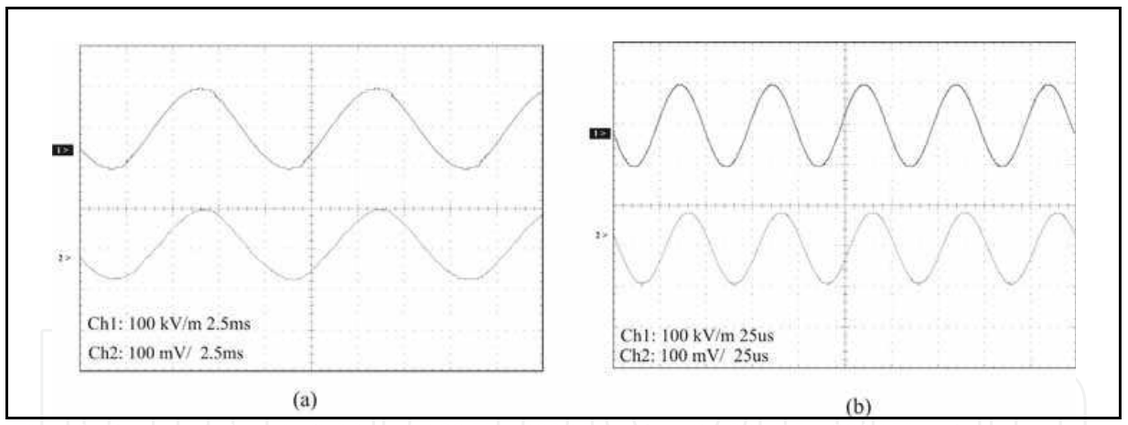

Fig. 13. Detected electric fields: (a) 100 Hz, 200 kVpp/m; (b) 20 KHz, 200 kVpp/m.

The minimum detected electric field was determined experimentally by decreasing the intensity of the sensed electric field. As given by expression 17, the half-wave electric field depends on the length of the electrooptic sensor. A longer sensor will be more sensitive and the minimum detected field will be lower. Figure 14 depicts measurements for two crystal lengths; figure 14(a) shows the minimum detected signal for a 13 mm length sensor when an 18 kVpp/m electric field is sensed. For comparison, 14(b) shows the recuperated signal for the same applied electric field when using a 36 mm sensor. These measurements indicate that for same sensed electric field, the sensitivity of the shorter sensor is significantly lower

than for the longer one; this is concluded by comparing the recuperated amplitude in both cases (14 mVpp and 60 mVpp, respectively), which corresponds to a ratio of about 13 dB.

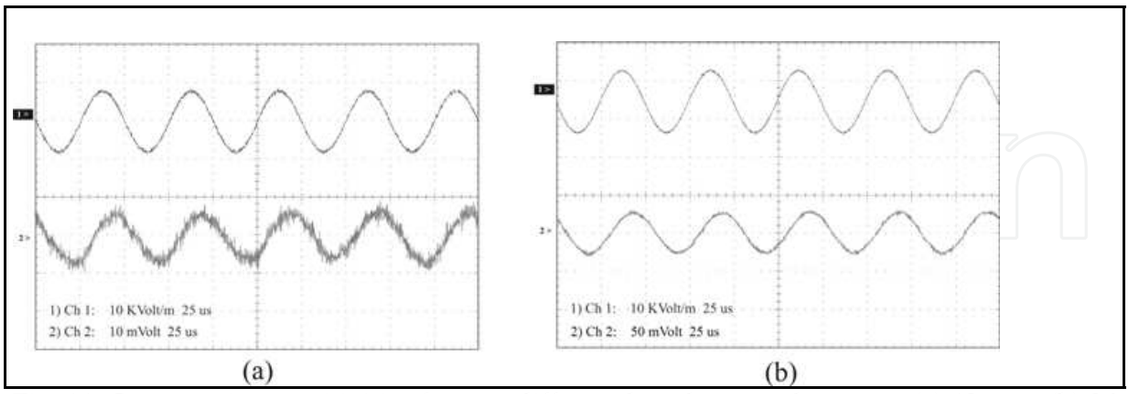

Fig. 14. Comparative sensitivities for two different lengths crystal sensors: (a) 13 mm; (b) 36 mm

5.2 Coherence multiplexed electric field sensing schemes

To explore novel applications of electro-optic sensors and coherence modulation of light, in this section an experimental coherence-multiplexed electric field sensing system using $LiNbO_3$ electro-optic coherence is described. A serial coherence multiplexed architecture seems attractive as the scheme uses only one optical source and the multi-channel optical signal is transmitted through a single optical fiber. Such a simple scheme can be proposed for a distributed electric field sensing array. A serial coherence multiplexed sensing array is shown in figure 15.

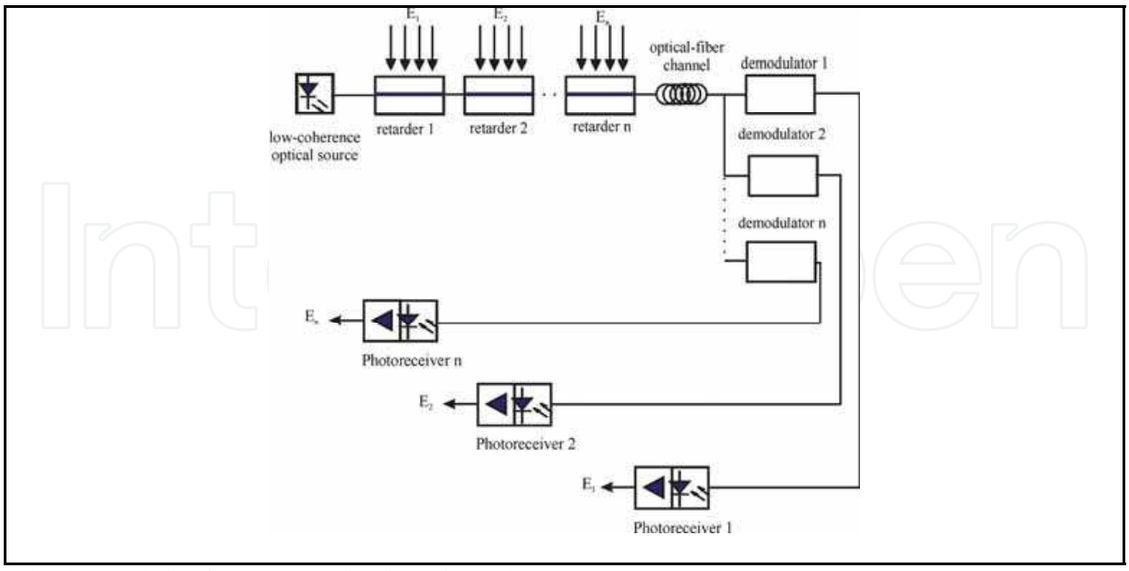

Fig. 15. Serial coherence multiplexed sensing array

The coherence modulated system described here represents an alternative to the classic

optical intensity measurement techniques and is additionally attractive as it can be used to implement serial coherence multiplexed sensor arrays, using only one optical source and a single optical channel.

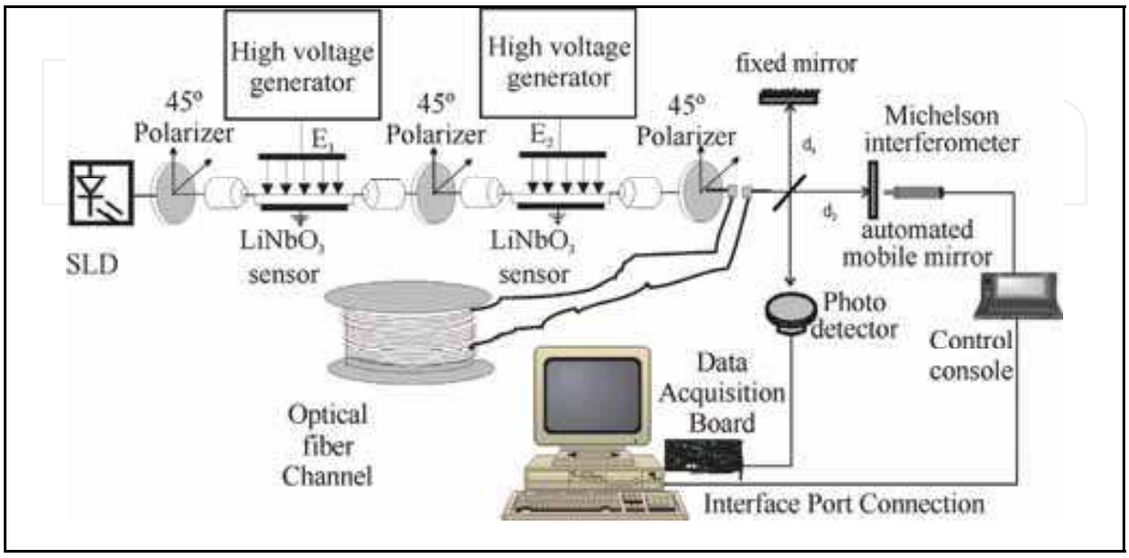

Fig. 16. Experimental two-channel coherence multiplexed electric field sensing scheme.

On the sensing side, light coming from the low-coherence optical source is injected into the first optical sensor, which introduces a first OPD. As explained before in this chapter, OPD's are generated by $LiNbO_3$ electro-optic sensors. The output of the first sensor becomes the input of the second one. At the output of the second stage, light exhibits two successive OPD's, that are modulated by two different electric fields.

For a two-channel transmission scheme (Goedgebuer et al, 1987; Gutiérrez-Martínez et al, 2002), from expression 1, the optical signal at the output of the first sensor introducing an optical delay τ_{01}, is given as

$$S_{m1}(t) = \frac{1}{2}\, s(t - \frac{\tau_{01}}{2}) + \frac{1}{2}\, s(t + \frac{\tau_{01}}{2}) \tag{21}$$

$s(t)$ is the low coherence optical signal coming from the SLD.

The optical signal given by expression 21, is the input to the second sensor, which introduces a second optical delay τ_{02}

$$S_{m2}(t) = \frac{1}{4}\left\{ s(t - \frac{\tau_{01}}{2} - \frac{\tau_{02}}{2}) + s(t - \frac{\tau_{01}}{2} + \frac{\tau_{02}}{2}) + s(t + \frac{\tau_{01}}{2} - \frac{\tau_{02}}{2}) + s(t + \frac{\tau_{01}}{2} + \frac{\tau_{02}}{2}) \right\} \tag{22}$$

At the output of the coherence demodulator (the Michelson interferometer), which introduces an optical delay τ, the received optical signal is

$$S_r(t) = \frac{1}{4}\left[S_{m2}(t - \frac{\tau}{2}) + S_{m2}(t + \frac{\tau}{2}) \right]$$

The corresponding detected optical intensities at the output of each channel are respectively

$$I_{r1,r2} = \left\langle S_{r1,r2}{}^{*}(t) S_{r1,r2}(t) \right\rangle$$

Finally, after some cumbersome mathematics, the detected optical intensities I_{r1} or I_{r2}, at the output of each channel, in terms of OPD's, are given as

$$I_{r1,r2}(d) = \frac{I_0}{16}\left[1 + g(d) + \frac{1}{2}g(d \pm d_{m01}) + \frac{1}{2}g(d \pm d_{m02}) + \frac{1}{4}g(d \pm (d_{m02} - d_{m01})) + \frac{1}{4}g(d \pm (d_{m02} + d_{m01}))\right] \tag{23}$$

I_0 is the average power of the optical source, d_{m01} and d_{m02} are the static OPD's for channels 1 and 2, $g(\bullet)$ is the normalized auto-correlation of the received optical field and $I_{r1,2}(d)$ are the received optical intensities at the output of the corresponding channels 1 or 2. Expression 23 represents a group of fringe patterns $g(d)$, located along the OPD axis. It can be observed that fringe patterns are located around zero, $\pm d_{m01}$, $\pm d_{m02}$, etc. As the optical path-differences d_{m01} and d_{m02} are greater than the coherence length l_c of the optical source, no interference occurs between the optical delays and a serial coherence-multiplexing process has been achieved. At the receiver, when the coherence demodulator is matched to each electrooptic sensor, only $g(d \pm d_{m01})$ or $g(d \pm d_{m02})$, will remain.

For implementing the two channel sensing scheme, the static optical path-differences of the coherence sensors were firstly measured. Figure 17(a) shows the auto-correlation fringe patterns of the cascaded coherence modulators. According to the $LiNbO_3$ crystal lengths, the introduced OPD's are of d_{m01} = 1.53 mm and d_{m02} =2.34 mm. These OPD's are modulated by the sensed electric fields. The electric fields can be detected at the receiver by adjusting the Michelson interferometer at OPD's $d_1 = (d_{m01} - \frac{\lambda_0}{4})$ and $d_2 = (d_{m02} - \frac{\lambda_0}{4})$. For a dynamic test of the sensing scheme, steady 60-Hz sinusoidal electric fields were generated and applied to the electro-optic sensors. The modulated light was transmitted through the 700 m optical fiber channel. The received light was then measured by the Michelson interferometer when adjusted in the linear region around the static optical path-differences.

The applied field was varied in the range 100-250 kVpp/m and in all cases, linear detection was achieved. Figure 17(b), illustrates the form of a 250 kVpp/m applied electric field and it also shows the detected voltages, which correspond to the detected electric field on each sensor channel. No cross-talk was observed between the two channels, as ensured by the continuous spectrum and low-coherence SLD optical source.

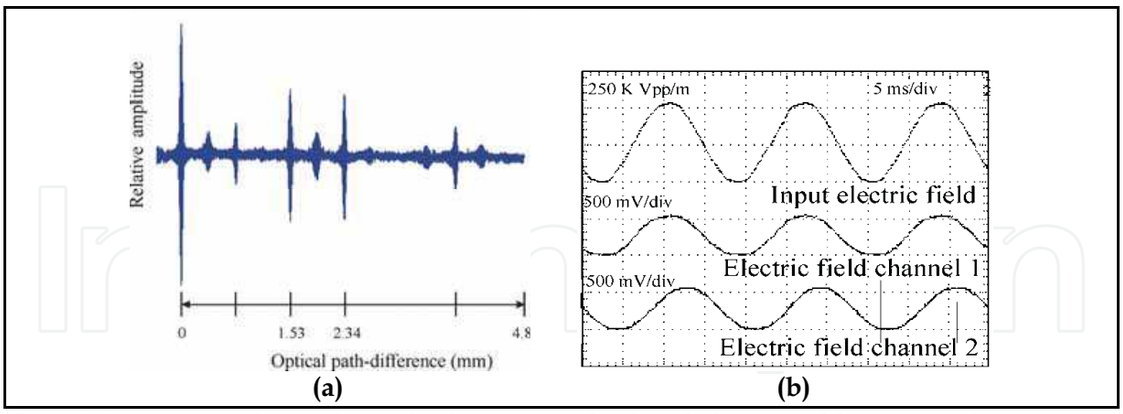

Fig. 17. Experimental two-channel coherence multiplexed electric field sensing scheme.

6. Wide-Band Electric Field Sensing

The frequency response of the studied electric field sensing schemes, is determined by the modulation sensitivity of the $LiNbO_3$ sensor, which depends on its high relative permittivity $\varepsilon_r = \sqrt{\varepsilon_{13}\varepsilon_{33}} = 35$, $\varepsilon_{13} = 44$ and $\varepsilon_{33} = 28$. As it has been well established on theoretical and experimental work (Kaminow & Liu, 1963; Rigrod & Kaminow, 1963; Nash & Smith, 1968; Chen, 1978), the frequency response will depend on the nature of the interaction between the electric and optical fields. If the electric field is applied via lumped electrodes, by using parallel plates, the frequency response is a trade-off of the optical-electrical interaction length, in this case the crystal length L, as given by

$$f_m \bullet L = \frac{c}{\pi\sqrt{\frac{1+\sqrt{\varepsilon_{13}\varepsilon_{33}}}{2}}} \tag{24}$$

Such a response is equivalent to around 2.2 GHz-cm.

Sensing high frequency electric fields is an important issue, as a lot of human activities are related to the generation, transmission and use of electromagnetic energy. In electric power facilities, telecommunications, medicine, etc., electric fields are present and under particular circumstances they can become harmful for equipments, facilities, operators and users. High frequency electric fields are attracting attention as their effects on security and health are no yet well known.

Research in progress aims to sense multi-MHz electric fields using coherence electrooptic sensors. In the previous section of this chapter, 20 KHz electric field sensing has been described. However, sensing schemes for high intensity fields in frequencies up to 10 MHz, are being studied. In a recent experiment, a dynamic 0-1 MHz signal has been generated by a video high voltage amplifier, producing an electric field adapted to the sensing range in the linear regions of the previously described schemes. The experimental set-up has already been tested for signals up to some hundreds of KHz. Measurements of 50 and 100 KHz electric fields are shown in figures 18 (a) and (b). The upper signal in each figure corresponds to the input signal to the wide band amplifier. The lower curve corresponds to the sensed electric field at the output of an available 100 KHz-bandwidth photoreceiver.

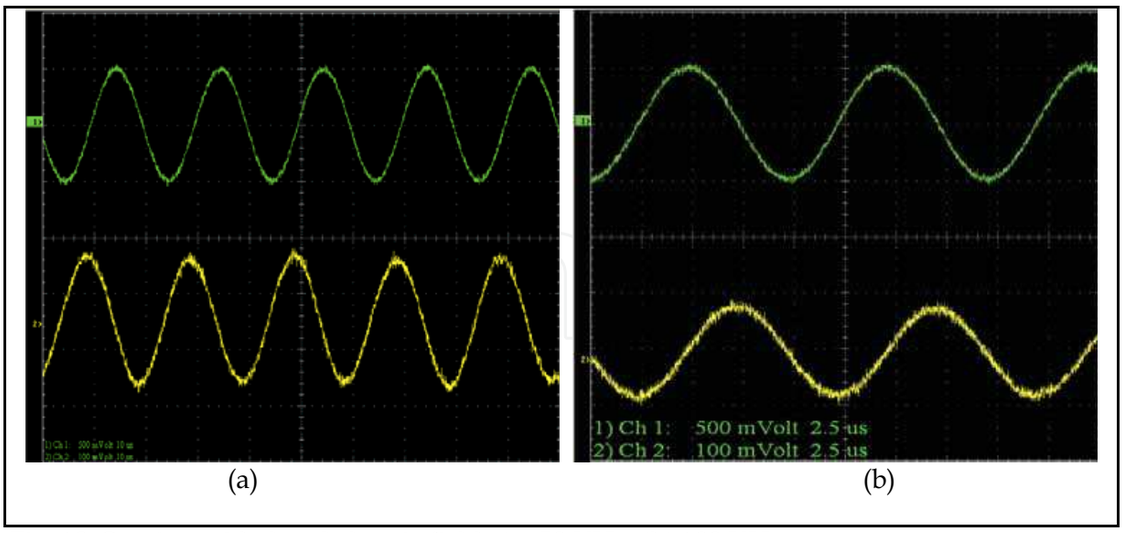

(a) (b)

Fig. 18. Sensing wide-band electric fields (a) 50 KHz; (b) 100 KHz.

The electric field range in these first results is of about 50 kVpp/m. Work is in progress for optimizing high-sensitivity photoreceivers for detecting video signals in the range of some tenths of MHz.

7. SNR performance

An important parameter for evaluating the electric field sensing system performance is the signal to noise ratio (SNR), which determines the minimun detectable electric field. The SNR is limited by noise (spontaneous beat, thermal and shot) at the photodetection process (Derickson, 1998; Killen, 1991; Hall, 1973).
At the receiver, the instantaneous photodetected current is of the form

$$I(t) = RP_r(1 + m\cos\omega_m t) \tag{25}$$

$R = \frac{\eta q}{h\nu}$ is the optical responsivity ($\eta = 0.7$) is the quantum efficiency, q is the charge unit, h is the Planck constant and ν is the optical frequency; P_r is the received optical power and m is the modulation index ($m = \frac{\pi E_{z0}}{2E_\pi}$).
The total photodetected current can be expressed as

$$I = I_{dc} + I_p(t) \tag{26}$$

$I_{dc} = RP_r$ is the average photocurrent and $I_p(t)$ is the signal current with mean square value $\langle I_p^2 \rangle = \frac{1}{2} m^2 R^2 P_r^2$.
The overall SNR is then given as

$$SNR = \frac{\langle I_P^2 \rangle}{RIN R^2 P_r^2 B + 2qI_{dc}B + \frac{4kTB}{\mathrm{Re}}} \tag{27}$$

In this expression, $RIN \bullet R^2 P_r^2 B$ corresponds to the beat noise power, $2qI_{dc}B$ is the shot noise power and $\frac{4kTB}{\mathrm{Re}}$ is the thermal noise power. RIN is the relative intensity noise of the optical source, k is the Boltzmann constant, T is the absolute temperature, B is the electrical bandwidth and Re is the equivalent load resistance of the photodetector.

To evaluate the SNR, the three main noises are considered. The beat noise, related to RIN, comes from the incoherent optical source whereas the shot and thermal noise are associated to the photodetection process (Derickson 1998; Killen, 1991; Andonovic & Uttamchandani, 1989; Baney et al, 1994; Baney & Sorin, 1995; Obarski & Hale, 1999).

In our experimental sensing schemes, the noise sources are related to the characteristcs of the optical source, the photodetector and the associated electronic amplifier. The optical source is a broadband SLD, emitting a gaussian spectrum centered at λ_0 =1310 nm and spectral width $\Delta\lambda$ =60 nm. The received average optical power is of about 0.5 μW and the electrical bandwidth on the photoreceiver is B=20 KHz. After the theoretical basis, such a gaussian optical source will exhibit a maximum $RIN = \frac{0.66}{\Delta\nu}$. $\Delta\nu = \frac{c\Delta\lambda}{\lambda_0^2}$ being the optical bandwidth. For the SLD the RIN is of about -132 dB/Hz. This corresponds to a spontaneous beat noise power of about -188 dBm. A similar calculation, regarding the shot noise power, gives -176 dBm.

When supposing that our system is only shot noise limited, the signal to noise ratio is

$$SNR = \frac{\eta m^2 P_r}{2h\nu B}$$

The minimum detectable external electric field is obtained when SNR=1.

$$E_{z\min} = \varepsilon r \frac{4}{\pi} \sqrt{\frac{2h\nu B}{\eta P_r}} E_\pi \ (\mathrm{Vpp/m}) \tag{28}$$

From this expression, for an $LiNbO_3$ sensor crystal of 13 mm in length and permittivity εr =35, the minimum detected external electric field, in agreement to expression 19, is of about 2 kVpp/m. For a crystal of 35 mm and the same optical parameters, the minimum detected field is of 0.7 kVpp/m. This theoretical calculation shows that sensitivity on the electrooptic sensors, depends strongly on the crystal dimensions. The longer crystals will present lower half-wave electric fields and hence higher sensitivities. In practical applications, the longest crystals are of around 75 mm (3 inches), limited by the size of LiNbO3 commercial wafers.

8. Conclusion

Optical coherence modulation of light using $LiNbO_3$ electrooptical retarders and low coherence optical sources for electric filed sensing schemes have been described in this chapter. The described principles were applied in experimental fiber and integrated optics

coherence-modulated optical schemes for sensing audio frequency electric fields. The detection of high-intensity electric fields, ranging form 10 to 350 kVpp/m and 0 to 20 kHz respectively, based on matched optical retarders, has been successfully tested in our laboratory. Work is in progress to achieve larger bandwidths, e.g., in the Megahertz range. In this kind of sensing schemes, the bandwidth is only limited by the light transit time on the electro-optic sensor. $LiNbO_3$ electro-optic devices are inherently very wide-band, responding potentially from DC to several GHz. The relative high-intensity operating range of our experimental scheme is determined by the use of short electro-optic crystals as the half wave electric field is high. As demonstrated in the experimental results, longer crystals allow lower half-wave fields and hence the measurement of lower intensity electric fields.

Sensing electric fields based on coherence modulation is a relatively novel approach and several aspects need to be investigated before becoming a real technical alternative for practical applications. It is very well known that fiber polarizers and the electro-optic birefringent sensors are sensitive to environmental variations. In particular, these elements are sensitive to temperature changes that affect their performances and potential long term drift can be observed on the sensor and demodulator operating points. In our experimental set-up no drift has been observed even if the system has been operating for several hours a day. However this drift may exist as it is inherent on the devices we used in our experimental work. To overcome the potential temperature dependence on the electro-optic crystals, polarization-independent electro-optic devices are being studied. Such devices much less are polarization sensitive and can be promising to implement more performant electric field sensing schemes. Work in such a direction is in progress in our laboratory.

The described sensing schemes represent potential applications of wide-band coherence-modulated sensors in more complex schemes, involving optical multiplexing to give distributed arrays of sensors, based on matched electro-optic sensors and demodulators, in fiber optics architectures. A fiber serial coherence multiplexing, in a simple array implementation could be useful for detecting and analyzing multi-point electric fields in the electric power industry, in high-intensity electric-fields environments, for high intensity telecommunication signals, etc.

9. References

Johnston, A. R.; Kirkham, H. & Eng B. T. (1986). Dc electric field meter with fiber optic readout. *Rev Sci. Instrumn*, vol. 57, No. 11, (November 1986)(2746-2753).

Kirkham, H. (2006). Measuring Electric Fields from Power Lines: Part 1. *IEEE Instrumentation and Measurement Magazine*, Vol. 9, No. 3, (June 2006)(54-56).

Kirkham, H. (2006). Measurement of Electric Fields Generated from Alternating Current. *IEEE Instrumentation and Measurement Magazine*, Vol. 9, No. 5, (October 2006)(58-61).

Kirkham, H. (2006). Dust Devil and Dust Fountains: The measurement Challenges. *IEEE Instrumentation and Measurement Magazine*, Vol. 9, No. 6, (December 2006)(48-52).

Harland, C. J. ; Clark, T. D. & Prance, R. J. (2002). Remote detection of human electroencephalograms using ultrahigh input impedance electric potential sensors. *Applied Physisc Letters*, Vol. 81, No. 17, (21 october 2002)(3284-3286).

Meier, T.; Kostrzewa, C.; Petermann, K. & Schuppert, K. B. (1994). Integrated Optical E-Field Probes with Segmented Electrodes. *IEEE Journal of Lightwave Technology*, Vol. 12, No. 8, (August 1994) (1497-1503).

Rao, Y. J.; Gnewuch, H.; Pannell, C. N. & Jackson, D. A. (1999). Electro-optic electric field sensor based on periodically poled $LiNbO_3$. *Electronics Letters*, Vol. 35, No. 7, (1st April 1999)(596-597).

Yim, Y-S.; Shin, S-Y.; Shay, W-T & Lee, Ch-T. (1998). Lithium niobate integrated-optic voltage sensor with variable sensing ranges. *Optics communicationss*, Vol. 152, (1 july 1998)(225-228).

Lee, T-H.; Hwang, F-T.; Shay, W-T & Lee, Ch-T. (2006). Electromagnetic Field Sensor Using Mach-Zehnder Waveguide Modulator. *Microwave and Optical Technology Letters*, Vol. 48, No. 9, (9 September 2006)(1897-1899).

Hidaka, K. & Fujita, H. (1982). A new method of electric field measurement in corona discharge using Pockels device. *Journal of Applied Physics*, Vol. 53, No. 9, (September 1982)(5999-6003).

Naghski, D. H. ; Boyd, J. T.; Jackson, H.; E. Sriram, S.; Kingsley, S. A. & Latess, J.(1994). An integrated Photonic Mach-Zehnder Interferometer with No-Electrodes for Sensing Electric Fields, *IEEE Journal of Lightwave Technology*. Vol. 12, No. 6, (June 1994)(1092-1097).

Cecelja, F.; Bordovsky, M. & Balachandran, W. (2001). Lithium Niobate Sensor for Measurement of DC Electric Fields. *IEEE Transactions on Instrumentation and Measurement*, Vol. 50, No. 2, (April 2001)(465-469).

Delisle, C. & Cielo, P. (1975). Application de la modulation spectrale à la transmission de l'information", *Can. J. Phys.*, 53, (1975)(1047-1053).

Brooks, J. L. & Wentworth, R. H. (1985). Coherence multiplexing for fiber-optic interferometric sensors. *IEEE J. Lightwave Technology*, vol. LT-3, (May 1985)(1062-1072).

Chu, K. W. & Dickey, F. M. (1991). Optical coherence multiplexing for interprocessor communications. *Opt. Eng.*, vol. 30, no. 3, (March 1991)(337-344).

Bock, W. J. & Urbanczyk, W. (2000). Coherence multiplexing of fiber-optic pressure and temperature sensors based on highly birefringent fibers. *IEEE Trans. On Instrumentation and Measurement*, vol. 49, no. 2, (April 2000)(392-397).

Porte, H. & Goedgebuer, J. P. (1992). An $LiNbO_3$ Integrated Coherence Modulator. *J. Lightwave Technology*, vol.10. No.6, (June 1992).

Gutiérrez-Martínez, C.; Porte, H. & Goedgebuer, J. P. (1995). Microwave Integrated Optics $LiNbO_3$ Coherence Modulator for High-Speed Optical Communications. *Microwave Opt. Technol. Lett.*, vol. 10, no. 1, (Sep. 1995)(62-66).

Rodríguez-Asomoza, J. & Gutiérrez-Martínez, C. (2001). Electric Field Sensing System Using a Ti: LiNbO3 Optical Coherence Modulator", *Proceedings of IEEE-International Measurement Technology Conference* (IMTC01), pp. 1075-1078, May 2001, Budapest, Hungary.

Gutiérrez-Martínez, C.; Trinidad-Garcia, G. & Rodríguez-Asomoza, J. (2002). Electric Field Sensing System Using Coherence Modulation of Light. *IEEE Transactions on Instrumentation and Measurement*, Vol. 51, No. 5, (October 2002)(985-989).

Gutiérrez-Martínez, C. & Santos-Aguilar, J. (2004). Wide-band Electric Field Sensing System Using Coherence Modulation of Light", *Proceedings of IEEE-International*

Measurement Technology Conference (IMTC 2004), pp. 1882-1885, May 2004, Como, Italy.

Gutiérrez-Martínez, C.; Santos-Aguilar, J. & Ochoa-Valiente, R. (2007). An All-Fibre and Integrated Optics Electric Field Sensing Scheme Using Matched Optical Delays and Coherence Modulation of Light. *Measurement Science and Technology*, IOP Publishing, Vol. 18, No. 10, (October 2007)(3223-3229).

Gutiérrez-Martínez, C. & Santos-Aguilar, J. (2008). Electric Field Sensing Scheme Based on Matched LiNbO3 Electro-Optic Retarders. *IEEE Transactions on Instrumentation and Measurement*, Vol. 57, No. 7, (July 2008)(13625-1368).

Goedgebuer, J. P.; Porte, H. & Hamel, A. (1987). Electrooptic Modulation of Multilongitudinal Mode Lasers Diodes: Demonstration at 850 nm with simultaneous Data Transmission by Coherence multiplexing. *IEEE J. Quantum Electron*, Vol. QE-23. No. 7, (July 1987)(1135-1144).

Goedgebuer, J. P. & Hamel, A. (1987). Coherence multiplexing using a parallel array of electrooptic modulators and multimode semiconductors lasers. *IEEE J. Quantum Electron*, Vol. QE-23. No. 12, (1987)(2224-2237).

Gutiérrez-Martínez, C.; Porte, H. & Goedgebuer, J. P. (1997). A Microwave coherence-multiplexed optical transmission system on $Ti:LiNbO_3$ integrated optics Technology. *Microwave and optical technology letters*, Vol. 14. No.1, (1997).

Gutiérrez-Martínez, C. (1994). Multiplexage par Modulation de Cohérence en Optique Integrée sur Niobate de Lithium ($LiNbO_3$); Etude et Réalisation de Modulateurs Rapides de Cohérence. *PhD. Thesis*. 1994. U de Franche-Comté, Besancon, France.

Ulaby, F. T. (2000). Chapter 4, In: *Fundamentals of Applied Electromagnetics*, , Prentice Hall.

Gutiérrez-Martínez, C.; Sánchez-Rinza, B.; Rodríguez-Asomoza J. & Pedraza-Contreras, J. J. (2000). Automated measurement of optical coherence lengths and optical delays for applications in coherence modulated optical transmissions. *IEEE Trans. On Instrumentation and Measurement*, vol. 49, no. 1, (February 2000)(32-36).

Kaminow, I. P. & Liu, J. (1963). Propagation characteristics of partially loaded two-conductor transmission line for broadband light modulators. *Proceedings of the IEEE*, (January 1963)(132-135).

Rigrod, W. W. & Kaminow, I. P. (1963). Wide-band microwave light modulation. *Proceedings of the IEEE*, (January 1963)(137-140).

Nash, F. R. & Smith, P. W. (1968). Broadband optical coupling modulation. *IEEE Journal of Quantum Electronics*, (January 1968)(26-34).

Chen, F-S. (1978). Modulators for optical communications. *Proceedings of the IEEE*, Vol. 58. No.10, (October 1978)(1440-1457).

Derickson, D. (editor). (1998). Hewlett-Packard professional books: *Fiber optic test and measurement*, pp (246-283). Prentice Hall PTR. Upper Saddle River, NJ.

Killen, H. B. (1991). *Fiber optics communications*, pp (43-68). Prentice Hall PTR. Englewood Cliffs, NJ.

Hall, C. (1973). Questions and answers about noise in electronics, pp (17-68). Howard W. Sams & Co. Indianapolis, Indiana.

Andonovic, I. & Uttamchandani, D. (1989). *Principles of modern optical systems*, pp (109-120). Artech House. Norwood, Mass.

Baney, D. M.; Sorin, W. V. & Newton, S. A. (1994). High-frequency photodiode characterization using a filtered intensity noise technique. *IEEE Photonics Technology Letters*, Vol. 6, No. 10, (October 1994)(1258-1260).

Baney D. M. & W. V. Sorin, W. V. (1995). Broadband frequency characterization of optical receivers using intensity noise. *Hewlett-Packard Journal*, Vol. 46, (February 1995)(6-12).

Obarski G. E. & Hale, P. D. (1999). How to measure relative intensity noise in lasers. *Laser Focus World*, (May 1999)(273-277).

Optical Fiber New Developments
Edited by Christophe Lethien

ISBN 978-953-7619-50-3
Hard cover, 586 pages
Publisher InTech
Published online 01, December, 2009
Published in print edition December, 2009

The optical fibre technology is one of the hop topics developed in the beginning of the 21th century and could substantially benefit applications dealing with lighting, sensing and communication systems. Many improvements have been made in the past years to reduce the fibre attenuation and to improve the fibre performance. Nowadays, new applications have been developed over the scientific community and this book fits this paradigm. It summarizes the current status of know-how in optical fibre applications and represents a further source of information dealing with two main topics: the development of fibre optics sensors, and the application of optical fibre for telecommunication systems.

InTech Europe
University Campus STeP Ri
Slavka Krautzeka 83/A
51000 Rijeka, Croatia
Phone: +385 (51) 770 447
Fax: +385 (51) 686 166
www.intechopen.com

InTech China
Unit 405, Office Block, Hotel Equatorial Shanghai
No.65, Yan An Road (West), Shanghai, 200040, China
中国上海市延安西路65号上海国际贵都大饭店办公楼405单元
Phone: +86-21-62489820
Fax: +86-21-62489821

IntechOpen